Title

Injectable borax-loaded alginate hydrogels reduce muscle atrophy, inflammation and generate neuroprotection in the SOD1G93A mouse model of ALS

Ana Rodríguez-Romano[1,2], Juan Gonzalez-Valdivieso[2,3], Laura Moreno-Martinez [4,5], Juan Francisco Vázquez Costa[6,7], Rosario Osta[4,5], Patricia Rico[1,2].*

[1] Biomedical Research Networking Center in Bioengineering, Biomaterials and Nanomedicine (CIBER-BBN)

[2] Center for Biomaterials and Tissue Engineering (CBIT)

Universitat Politècnica de València

46022 Valencia, Spain

[3] Universidad de Valladolid

47002 Valladolid, Spain

[4] Biomedical Research Networking Center in Neurodegenerative Disorders (CIBERNED)

[5] LAGENBIO-I3A, Veterinary Faculty of Zaragoza, Aragonese Institute of Health Sciences (IACS).

University of Zaragoza

50013 Zaragoza, Spain.

[6] Biomedical Research Networking Center on Rare Diseases (CIBERER)

[7] Neuromuscular Unit

Hospital Universitario y Politécnico la Fe, IIS La Fe

46026 Valencia, Spain.

Dr P. Rico, PhD *corresponding author

[1]Biomedical Research Networking Center in Bioengineering, Biomaterials and Nanomedicine (CIBER-BBN)

[2]Center for Biomaterials and Tissue Engineering (CBIT).

Universitat Politècnica de València

46022 Valencia, Spain

E-mail: parico@upvnet.upv.es

Abstract

Amyotrophic Lateral Sclerosis (ALS) is the most frequent and fatal condition that causes motor neurons loss and skeletal muscle paralysis. Although ALS is associated with mutations in over 40 genes, its etiology remains elusive without a cure or effective treatment. Historically considered the prototype of motor neuron diseases, ALS is defined today as a multisystem disorder that presents several changes in non-neuronal cell types, such as pathological changes in muscle occurring before disease onset and independent from motor neuron degeneration (dying back hypothesis). We based in the hypothesis that skeletal muscle may have an active contribution to disease pathology and thus we consider skeletal muscle tissue as a therapeutic target for ALS.

In previous works we have demonstrated that borate (B) transporter NaBC1 (encoded by *SLC4A11* gene), after activation co-localize with integrins and growth factor receptors producing a functional cluster that synergistically enhances crosstalk mechanisms accelerating muscle repair. In this work we aimed to study the effects of B in a SOD1 mouse model of ALS targeting muscle. We have engineered and characterized injectable alginate-based hydrogels with controlled local borax-release for an effective activation of NaBC1 *in vivo*. Treated mice presented improved motor function and extended survival that was correlated with an enhanced muscle repair response inducing a reduction in muscle atrophy and inflammation. Interestingly, the activation of muscle repair mechanisms at local level, produced a retrograde neuroprotection by motor neuron preservation and reduction in neuro-inflammation. Altogether, this work presents evidence supporting the involvement of muscle tissue in ALS pathology, reinforcing skeletal muscle as a primary target to develop new therapies for ALS. We propose a novel strategy based on NaBC1 activation for ALS muscle regeneration.

Keywords

Borax, ALS, muscle regeneration, NaBC1 transporter (*SLC4A11*), alginate hydrogel.

1. Introduction

Amyotrophic Lateral Sclerosis (ALS) is the most frequent and fatal entity affecting motor neurons[1]. While the majority of ALS cases are sporadic, about 10% of the cases exhibit familial traits characterized by autosomal dominant inheritance. Clinical manifestations in both sporadic and familial ALS are indistinguishable, suggesting the convergence of diverse pathways in neuromuscular degeneration. Despite the identification of over 40 genes associated with ALS (https://alsod.ac.uk/), the aetiology of ALS remains elusive, with no cure or effective treatment available, only multidisciplinary care[2].

The primary challenge in comprehending the pathogenesis of ALS lies in the remarkable clinical heterogeneity of the disease phenotype and course, even among patients harboring the same mutation[3,4]. Additionally, the multisystemic nature of ALS pathology, spanning various biological systems, further complicates the identification of a suitable therapeutic target.

Although ALS has been historically considered the prototype of motor neuron diseases, it is now defined as a multisystem disorder involving changes in non-neuronal cell types. A growing number of clinical and animal/cellular studies suggests that motor neuron damage may arise from mechanisms exhibited by glia[5] or muscle cells[6]. Strong evidence supports the “dying back” hypothesis indicating that pathology originates in skeletal muscle and transmits to the soma before the onset of clinical symptoms and motor neuron death[7,8]. Muscle-nerve interactions during muscle repair are essential to preserve muscle motor function, and skeletal muscle shows a key role in these events by secreting specific factors during regeneration. The observations of pathological changes in muscle preceding disease onset and independent of motor neuron degeneration highlights the

significance of focusing on muscle tissue in ALS research and underscores its potential as a target for ALS therapies[9].

Active areas of development of therapies for the treatment of muscle and motor neuron atrophy are based in the use of growth factors (GFs) either soluble[10], over expressed in mouse models[11] or stem cell-based growth factor delivery targeting glial cells[12] and muscle inflammation[13]. Nevertheless, only limited reports detail material systems designed for ion delivery as a bioactive elements to activate intracellular signaling.[14-17] Still there is a need to innovate and establish new methods and materials that facilitate the repair and functional regeneration of skeletal muscle.

Ions are capable of stimulating intracellular signaling, and some have potential as proangiogenic factors[17] opening a new avenue for their application in tissue engineering. Muscle atrophy is also often related to defects in cytosolic calcium homeostasis due to oxidative-stress, and thus targeting the calcium leakage from the muscle cells is other approach followed to improve muscle function[18,19]. Boron (B) plays a key role in mammalian cells in several metabolic pathways and in combination with other ions such as Ca^{2+} and Mg^{2+} as well as steroid hormones[20,21], however although B is essential in metabolism of mammalian cells[22] little is known about B homeostasis and function in cells.

The borate transporter NaBC1 (encoded by the *SLC4A11* gene), controls B homeostasis and functions as a Na^{+}-coupled borate co-transporter.[23] Only recently we have demonstrated a novel function for NaBC1 besides controlling borate homeostasis that after activation co-localize with integrins and growth factor receptors (GFRs) producing a functional cluster that synergistically enhances biochemical signals and crosstalk mechanisms enhancing vascularization[24], adhesion-driven osteogenesis[25], and muscle regeneration.[26,27]

In the present study, and based in our previous works, we investigated in a local proof of concept, the therapeutic efficacy of borax release from injectable alginate hydrogels targeting ALS muscle. We have used the SOD1 mouse model which recapitulates lower motor neuron degeneration, and muscle denervation atrophy occurs prior any evident sign of neurodegeneration.[7,28] We found that only four injections of the treatment administered in mice quadriceps prior symptoms onset, significantly improved motor function. This intervention also effectively reduced muscle atrophy, delaying symptom onset and extending mice survival. These positive outcomes were closely associated with muscle satellite cells activation and further progress through the myogenic program, crucial events for muscle regeneration and repair. Activation of NaBC1 potentiated muscle repair processes, resulting in the reduction of several pathological features characteristic of ALS-afflicted muscles and a decrease in muscle inflammation. Moreover, our data revealed that the recovery of muscle pathology had a retrograde neuro-protective effect, modulating neuro-inflammation and mitigating the loss of motor neurons. These findings play a crucial role in understanding the involvement of muscle tissue in ALS pathology, highlighting skeletal muscle as a primary therapeutic target. We propose a novel strategy based on the unique mode of action of active-NaBC1 to explore innovative treatments for ALS muscle regeneration.

2. Results and Discussion

2.1. Local borax-release preserves motor function, delays symptoms onset, and prolongs survival in a SOD1^{G93A} mouse model.

In this work we aimed to assess the effects of borax (B), as a local proof of concept, in an ALS murine model (B6SJL-Tg (SOD1^{G93A}) 1 Gur/J ALS) to evaluate the possible effects of B in the recovery of the pathological conditions of muscle and nerve inflammation caused by ALS degeneration. To do that, we engineered and characterized injectable

alginate-based hydrogels with controlled local B-release as previously described[27]. We loaded the hydrogels by a simple mixing procedure that can be easily translated to the clinic, with borax 0.15 M equivalent to 6 mg per 100 µL hydrogel (ALG-B). **Figure S1-a** shows the non-cumulative B-release of 6 mm injectable hydrogels. Release from ALG-B hydrogels resulted in approximately 1,200 mg L^{-1} at day 1, despite the initial loading of 6,000 mg L^{-1} indicating that part of the borax content remains entrapped within the hydrogel and becomes sustained released over time. **Figure S1-b** illustrates the percentage of borax-released corresponding to approximately 20 % of borax after 1 day.

SOD1 ALS male and female mice were randomly distributed and organized in two parallel experiments: i) pre-symptomatic mice: ALS control, ALS injected with empty hydrogel (ALS ALG) and ALS injected with treatment (ALS ALG-B). Mice were injected biweekly at 68 days old (before symptoms onset), 82, 96 and 110 days old and sacrificed at 115 days old. ii) symptomatic mice for survival assessment: ALS control and ALS injected biweekly with treatment (ALS ALG-B) at 68, 82, 96 and 110 days old and sacrificed upon reaching the final stage of disease progression-associated symptoms (between 120-146 days).

For each case, 100 µL of either saline solution (for the control groups) or ALG hydrogel (empty or B-loaded) was subcutaneously injected into the quadriceps muscles of all mice. Changes in body weight and motor impairment were tracked using a behavioral four-limb hanging test over a period of 12 weeks. One of the prominent characteristics of ALS in the $SOD1^{G93A}$ mutant mouse model is its ability to induce severe muscle atrophy, leading to a progressive loss of weight due to a reduction in muscle mass and a significant decline in muscle strength [29]. As depicted in **Figure 1-b**, the treated mice exhibited an increase in body weight over time, with the ALS ALG-B group demonstrating the most favorable

outcomes in the four-limb hanging test (Fig. 1-a) when compared to the non-treated control groups, suggesting preservation of motor function.

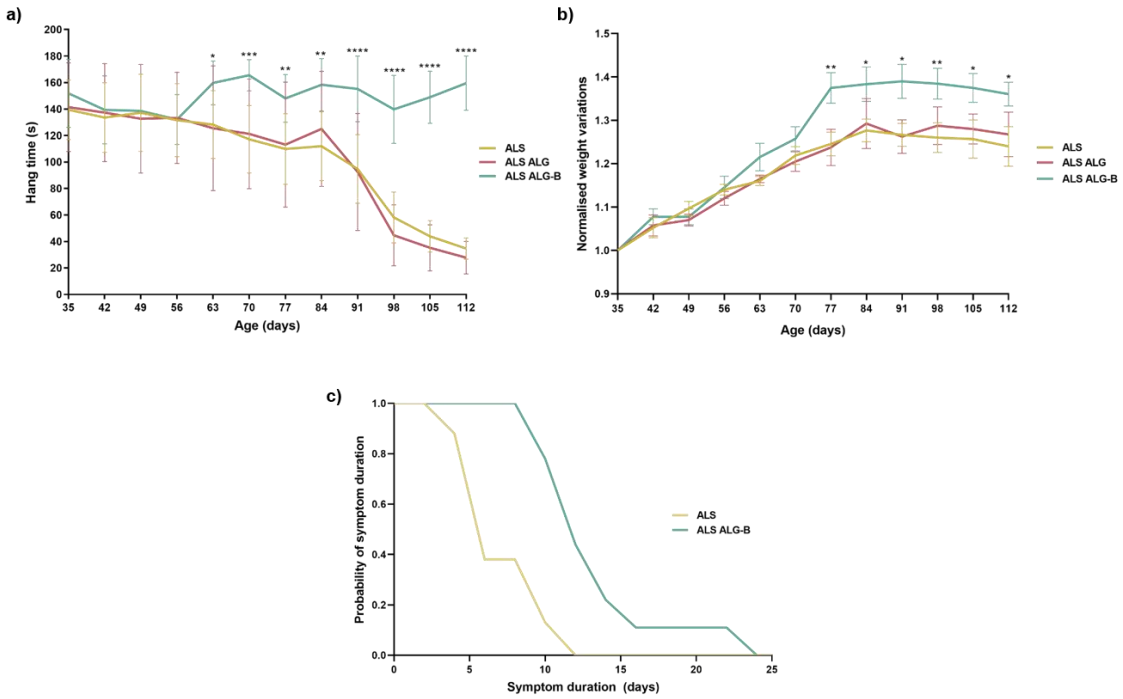

Figure 1. Evaluation of behavioral motor impairment and analysis of symptom duration

a, b) Changes over time in hanging time and weight of mice (male and female) distributed in the different groups (ALS, n = 6; ALG, n = 6; ALG-B, n = 6).

c) Probability of symptom duration comparison between the ALS (n = 10) and ALS ALG-B (n = 10) groups.

Statistics are shown as mean ± standard deviation. For comparison between the three groups, data were analyzed by an ordinary one-way ANOVA test and corrected for multiple comparisons using Tukey´s correction analysis (p = 0.05). Statistics indicate differences between groups. ****p < 0.0001, ***p < 0.001, **p < 0.01, *p < 0.05. For comparisons between two groups, data were analyzed by an unpaired t-test applying Welch´s corrections (p = 0.05).

Mutant SOD1^{G93A} mice with elevated copy numbers generally maintain good health until around 80-90 days of age, after which they manifest symptoms of motor neuron disease, including limb tremors during suspension. By 120 days, most of these mice progress to advanced disease stages, resulting in complete paralysis[30]. In addition to motor impairment, we monitored symptom progression in the survival (SV) experimental group. **Supplementary table 1** illustrates the onset, endpoint, and duration of symptoms in each group. Notably, the group treated with ALS ALG-B exhibited a delayed onset of symptoms and an extended survival period, approximately twice the duration of symptoms compared to the ALS control group (Fig. 1-c).

The observed improvement in motor function, along with the delay in symptoms onset and extended survival following local muscle treatment, suggests that muscle tissue may play a significant role in ALS pathology. This underscores the contribution of muscles to the pathological mechanisms affecting the disease, beyond motor neurons degeneration.

2.2. Local borax-release counteracts muscle atrophy in pre-symptomatic and symptomatic SOD1^{G93A} mice.

After euthanasia of pre-symptomatic and symptomatic mice, tissues were analyzed by histological techniques. The degeneration of muscle occurring after constant denervation and re-innervation processes, is characterized by a progressive muscle atrophy, in which the fibers appear as angular atrophic fibers, surrounded by compensatory hypertrophic fibers to maintain homeostasis,[31,32] and characterized by increased variability of fiber sizes, decreased fiber diameter and increased density of nuclear clumps between myofibres. For reliable quantification and measurement of pathology-relevant histological parameters of dystrophic muscle we have followed TREAT-NMD standard operating procedures (SOP). **Figure 2** shows histoarchitecture of muscle quadriceps

analyzed in pre-symptomatic and symptomatic mice. **Figure S2** shows an illustration of the segmentation process carried out in complete muscle tissue sections.

For fiber size determination we have employed the Feret´s diameter of muscle fibers cross-sections. This is a robust morphometric parameter that avoids experimental errors related to fiber orientation and sectioning angle. Moreover, reliably discriminates between dystrophic and normal phenotypes.

In both animal experiments, the ALS and ALG control groups displayed a decreased fiber size, a notable presence of atrophic fibers surrounded by hypertrophic fibers together with and increased density of nuclei, distinctly visible in the tissue sections (Figure 2, arrows) concordant with muscle atrophy appearing as a common feature of ALS. We also observed thickening of perimysium and endomysium, due to the augmented extracellular matrix components related to appearance of muscle fibrosis. Despite muscle ALS pathology was still evident, treated mice presented a noteworthy increase in the minimal Feret's diameter, suggesting an enlargement of muscle fibers. These results indicate the effective retardation of muscle atrophy progression by borax in both animal experiments, and corroborate treatment's effectiveness in promoting muscle growth or preventing further muscle degeneration, correlating with the obtained results showing an improved muscle function and strength after motor behavior evaluation (Fig.1).

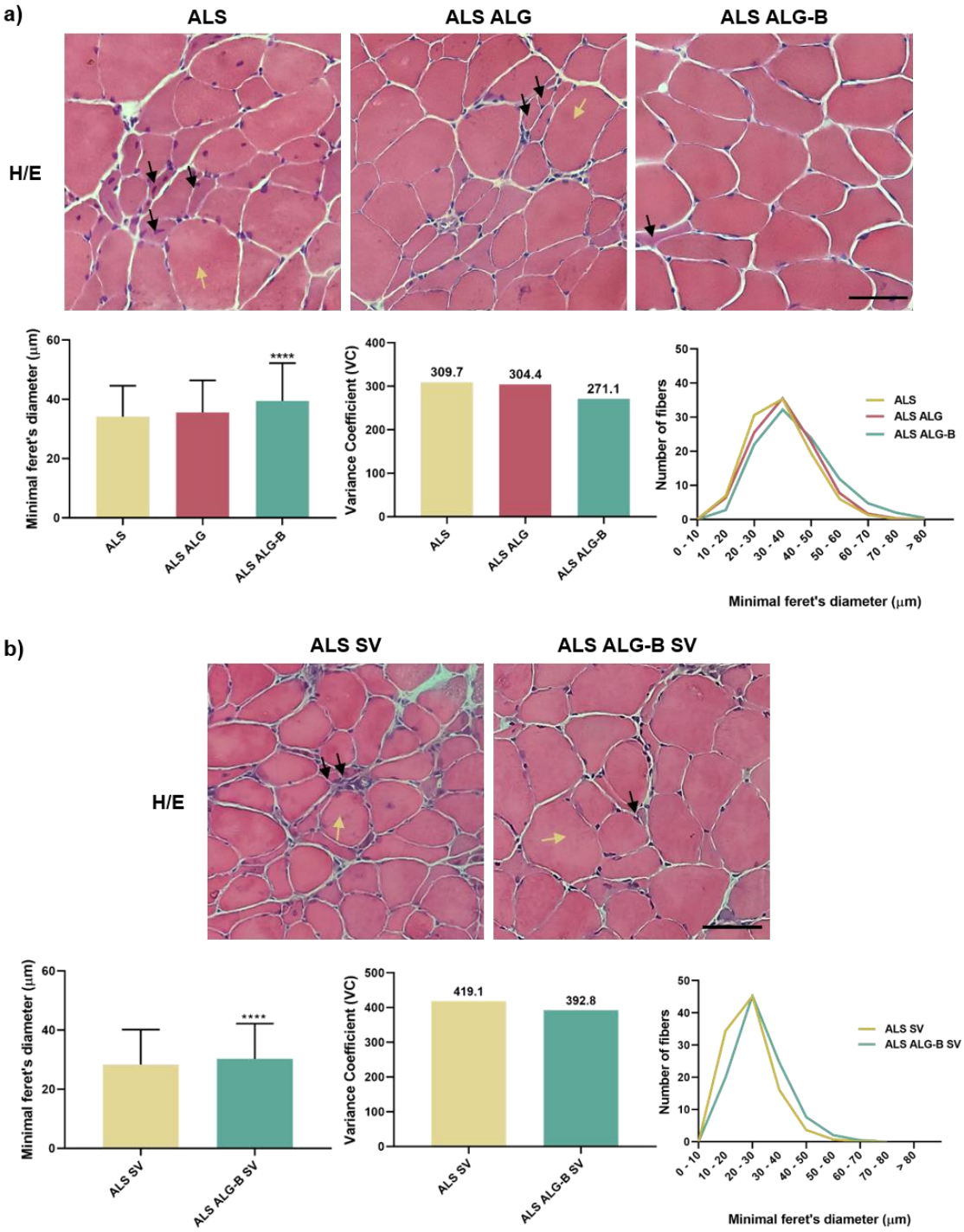

Figure 2. Morphometric muscle parameters in pre-symptomatic and symptomatic mice.

Histoarchitecture of pre-symptomatic (a) and symptomatic (b) muscle quadriceps visualized by hematoxylin/eosin staining. In both animal experiments, the ALG-B group displayed reduced muscle atrophy, as evidenced by a decrease in atrophic fibers (10-20

µm, black arrows) surrounded by hypertrophic fibers (50-60 µm, yellow arrows). Scale bar 50 µm. Image analysis quantification of morphometric parameters including minimal Feret´s diameter and variability among fibers (Variance coefficient, VC). The ALG-B group exhibited a significant increase in the minimal Feret's diameter and a decrease in VC, indicating a more uniform distribution of fiber sizes.

Statistics are shown as mean ± standard deviation. For comparison between the three groups, data were analyzed by an ordinary two-way ANOVA test and corrected for multiple comparisons using Tukey´s correction analysis ($p = 0.05$). For comparisons between two groups, data were analyzed by an unpaired t test applying Welch´s corrections ($p = 0.05$). ****$p < 0.0001$.

Furthermore, in both animal experiments, the ALG-B treated mice presented a reduction in the variability of fiber sizes, as expressed by the variance coefficient (VC), implying a decrease in the pathological characteristics present in ALS muscle. An analysis of the distribution of minimal Feret's diameters revealed that the ALG-B group had the highest number of fibers with increased minimal Feret's diameters. This finding is associated with an improved and accelerated regenerative response, indicating that the treatment is promoting muscle growth and function, and suggesting that some of the pathological features typically observed in ALS-afflicted muscles are mitigated.

The observation of reduced muscle atrophy in both pre-symptomatic and symptomatic mice suggests a lasting impact of borax treatment over time. Remarkably, just four injections of the treatment were sufficient to decelerate muscle atrophy progression, and these effects persisted until the end of the animals' lives, even though the animals still exhibited ALS pathology and ultimately succumbed to the disease, likely due to the extensive neurological damage.

2.3. Local borax-release preserves fast (type II) muscle fibers, augments satellite Pax7+ cells and reduces SOD1 and fibronectin levels in pre-symptomatic and symptomatic skeletal muscle of SOD1^{G93A} mice.

Skeletal muscle is characterized by a heterogeneous composition of two types of fibers. Type I (slow-twitch) fibers, optimized for endurance activities, have a high content of myoglobin, essential for providing instant oxygen, and abundant mitochondria. Type II (fast-twitch) fibers, are designed for short bursts of intense activity, have a major number of neuromuscular junctions and contain large amounts of glycogen as a source for anaerobic glycolysis.[33]

In ALS, muscle denervation is accompanied by a progressive replacement of type II by type I fibers. This phenomenon, reported in both murine models and patients, highlights the vulnerability of fast-twitch fibers, which predominantly exhibit an atrophic appearance, while slow-twitch fibers adopt a compensatory hypertrophic morphology.[31,32]

Immunofluorescence analysis of various muscle markers relevant to ALS is shown in **Figure 3**. Following borax treatment, we observed a substantial decrease in type I slow myofibers in the ALG-B muscle of both pre-symptomatic and symptomatic mice. Our findings suggest a potential preservation of type II fast myofibers. Given that type II fast fibers are the initial targets of atrophy in ALS, our results imply that the treatment is influencing the pathological myofiber transition characteristic of ALS. This aligns with our previous histological observations indicating a mitigation of muscle atrophy (Fig.2).

Several lines of evidence highlight the impact of ALS in muscle turnover, revealing that impaired myogenic processes could aggravate the denervation-induced muscle wasting. Muscle denervation re-innervation cycles occurring in ALS, are accompanied by satellite cell activation (Pax7+ cells) that play an essential role in the intrinsic repairing

mechanisms of muscle. ALS skeletal muscle satellite cells present impaired activity and myogenic potential. In ALS patients, Pax7 expression decreases[32] and satellite cells become activated but do not progress through the myogenic program exhibiting incomplete differentiation and abnormal myotube and senescent-like morphology.[34-36] In SOD1^{G93A} ALS mouse model, satellite cells exhibit compromised cell proliferation capacity, even during the pre-symptomatic disease stages along with a reduction in the number of Pax7+ cells.[37,38]

Figure 3 shows a significant increase in Pax7+ cells in ALG-B treated mice as compared to controls groups, evident in both pre-symptomatic and symptomatic stages. Notably, the percentage of Pax7+ cells in pre-symptomatic ALS control mice is higher than in symptomatic ALS control mice, underscoring the natural disease progression and validating previous reported observations indicating a decline in Pax7+ cells throughout the course of the disease.[37,38] Given the reduced number and compromised proliferation of satellite cells in the SOD1 model, our results indicating a substantial rise in active satellite cells suggest that borax is potentiating and enhancing muscle regeneration and repair processes. Our findings correlate with the observed improvements in muscle strength and overall motor function (Fig.1), indicating that satellite cells are not only active, but they are also effectively progressing through the myogenic program reflecting an enhanced capacity for muscle healing.

Furthermore, the observed increase in Pax7+ cells in symptomatic mice, who were in the advanced stages of the disease, indicate that treatment is offering long-term improvement potentially slowing down the progression of muscle degeneration.

We have also evaluated SOD1 (superoxide dismutase 1) and fibronectin (FN) expression at protein levels (Figure 3). SOD1 is a critical player of the anti-oxidative defense. The SOD1^{G93A} mouse model employed carries several copies of the human SOD1G93A

mutation (glycine to alanine at position 93) which results in a ubiquitous toxic gain of SOD1 function.[39,40] Specifically, skeletal muscle has been described as a primary target of $SOD1^{G93A}$-mediated toxicity on which oxidative stress triggers muscle atrophy.[29]

ALG-B treated pre-symptomatic and symptomatic mice presented a reduction in SOD1 protein levels indicating that treatment is helping to protect muscle from toxic SOD1 oxidative stress effects slowing down muscle deterioration, and conferring an improved muscle function and strength, which translate into the enhanced motor function observed in Fig.1 and reduction in muscle atrophy (Fig.2). Further investigation is needed to decipher the specific mechanism by which borax reduces SOD1 protein levels, even though our results suggest that ALG-B treatment is specifically targeting SOD1 within the muscle and could represent a promising therapeutic approach.

In addition, after muscle denervation processes, augmented FN protein levels have been reported in both ALS patients[41] and $SOD1^{G93A}$ mice,[42] related to the appearance of fibrotic changes. An active fibrotic process has been reported in skeletal muscle of symptomatic $SOD1^{G93A}$ mice.[42]

FN levels, were also diminished in pre-symptomatic and symptomatic mice after treatment, suggesting a reduction in muscle fibrosis levels related to FN overexpression.

Overall, our findings at protein level in muscle histopathology, align with the observed recoveries in motor function (Fig. 1) and the deceleration of muscle atrophy progression (Fig. 2) indicating that local borax treatment is exerting a positive impact on muscle integrity and function.

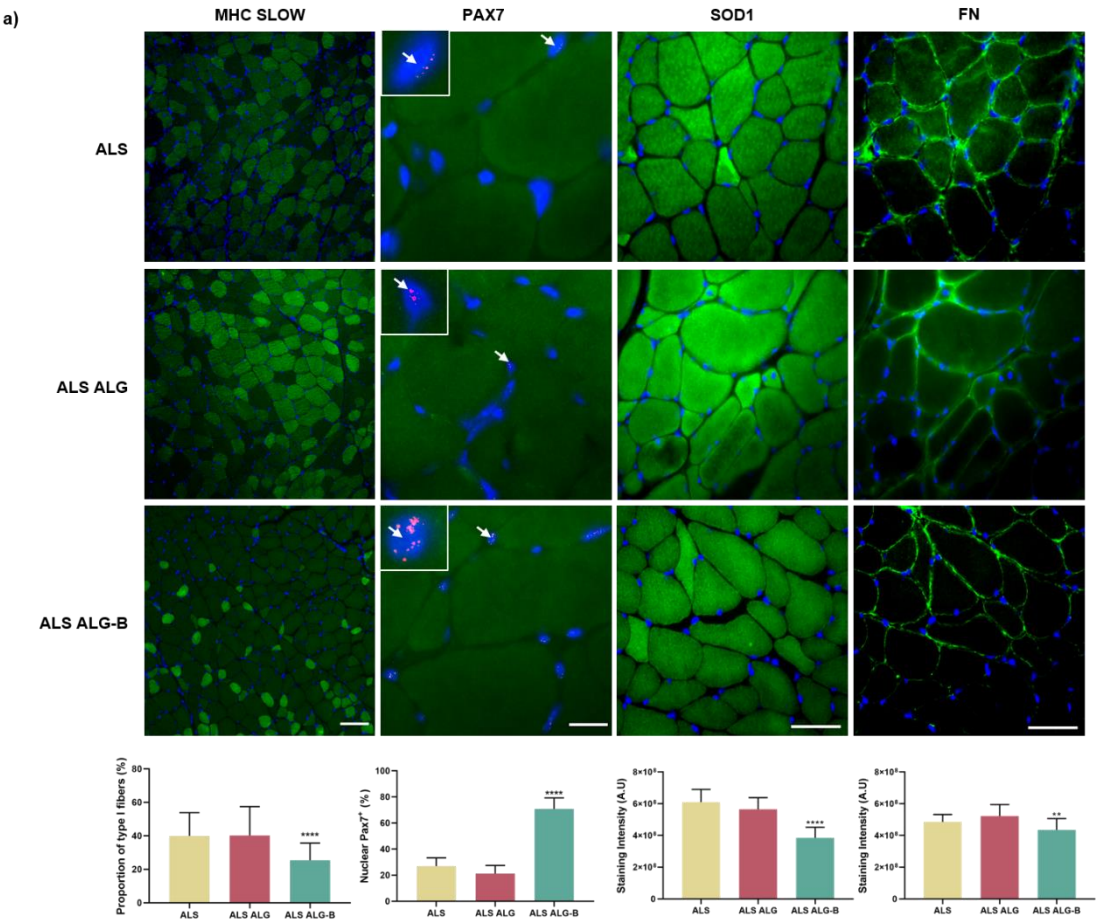
a)
MHC SLOW
PAX7
SOD1
FN
ALS
ALS ALG
ALS ALG-B
Proportion of type I fibers (%)
Nuclear Pax7+ (%)
Staining Intensity (A.U)
ALS
ALS ALG
ALS ALG-B

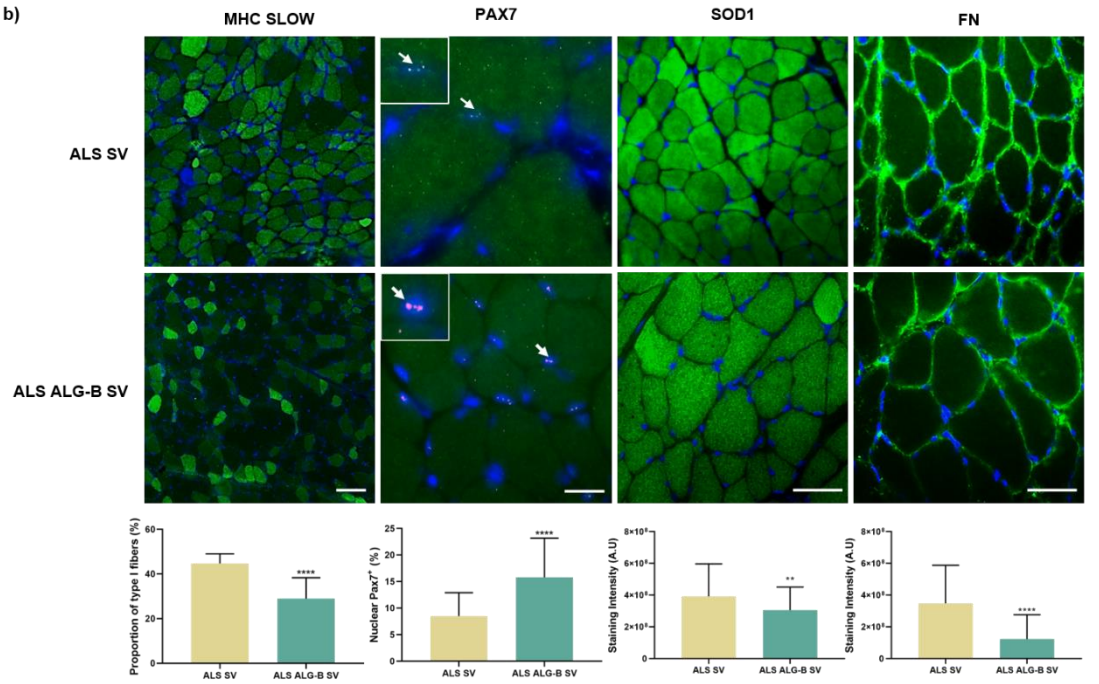
b)
MHC SLOW
PAX7
SOD1
FN
ALS SV
ALS ALG-B SV
Proportion of type I fibers (%)
Nuclear Pax7+ (%)
Staining Intensity (A.U)
ALS SV
ALS ALG-B SV

Figure 3. Immunofluorescence detection of ALS muscle markers in pre-symptomatic and symptomatic mice.

Immunofluorescence detection of slow type I fibers, Pax7+ satellite cells, SOD1 protein aggregates and fibronectin (FN). Quadriceps sections of pre-symptomatic (a) and symptomatic (b) mice were analyzed. In both animal experiments, the ALG-B group displayed reduced slow type I fibers, toxic SOD1 protein aggregates and FN levels, in line with the observation of a reduction of muscle atrophy after the treatment and with the increase in Pax7+ cells. Scale bar 50 µm. Graphs represent the image analysis quantification of the intensity of the different markers.

Statistics are shown as mean ± standard deviation. For comparison between the three groups, data were analyzed by an ordinary two-way ANOVA test and corrected for multiple comparisons using Tukey´s correction analysis ($p = 0.05$). For comparisons between two groups, data were analyzed by an unpaired t-test applying Welch´s corrections ($p = 0.05$). ****$p < 0.0001$, **$p < 0.01$.

2.4. Evaluation of muscle inflammation indicates that muscle borax-release reduces mast cell inflammatory response in pre-symptomatic and symptomatic SOD1^{G93A} mice.

In ALS, inflammation is as a key mechanism contributing to the degeneration process of both motor neurons and muscles. Several reports describe the presence of inflammatory cells within peripheral nerves and skeletal muscle of ALS patients and rodents.[43,44] Among inflammatory cells, the granulated hematopoietic-derived mast cells, activate upon tissue damage and orchestrate the inflammatory responses recruiting and activating other immune cells through degranulation and release of inflammatory mediators and enzymes,[45-48] mediating neurogenic inflammation.[49] Recent findings suggest that mast

cells directly interact with degenerating motor nerve endings and motor endplates in the skeletal muscle of SOD1^{G93A} rodents with their number and degranulation pattern correlating with the progression of paralysis,[43] highlighting their involvement in the chronic inflammatory muscle response in ALS. [50,51]

The evaluation of muscle mast cell recruitment revealed that in both, pre-symptomatic and symptomatic mice, the total infiltrated mast cell number was elevated in ALS and ALG control groups, even though the levels of de-granulated mast cells were extremely raised up in pre-symptomatic mice, indicating an active pro-inflammatory process concordant with the stage of progression of the disease. Accordingly, mast cells number in the periphery of nerve fibers was higher in symptomatic mice, indication of the extensive nerve inflammation characteristic of SOD1 mouse model (**Figure 4**).

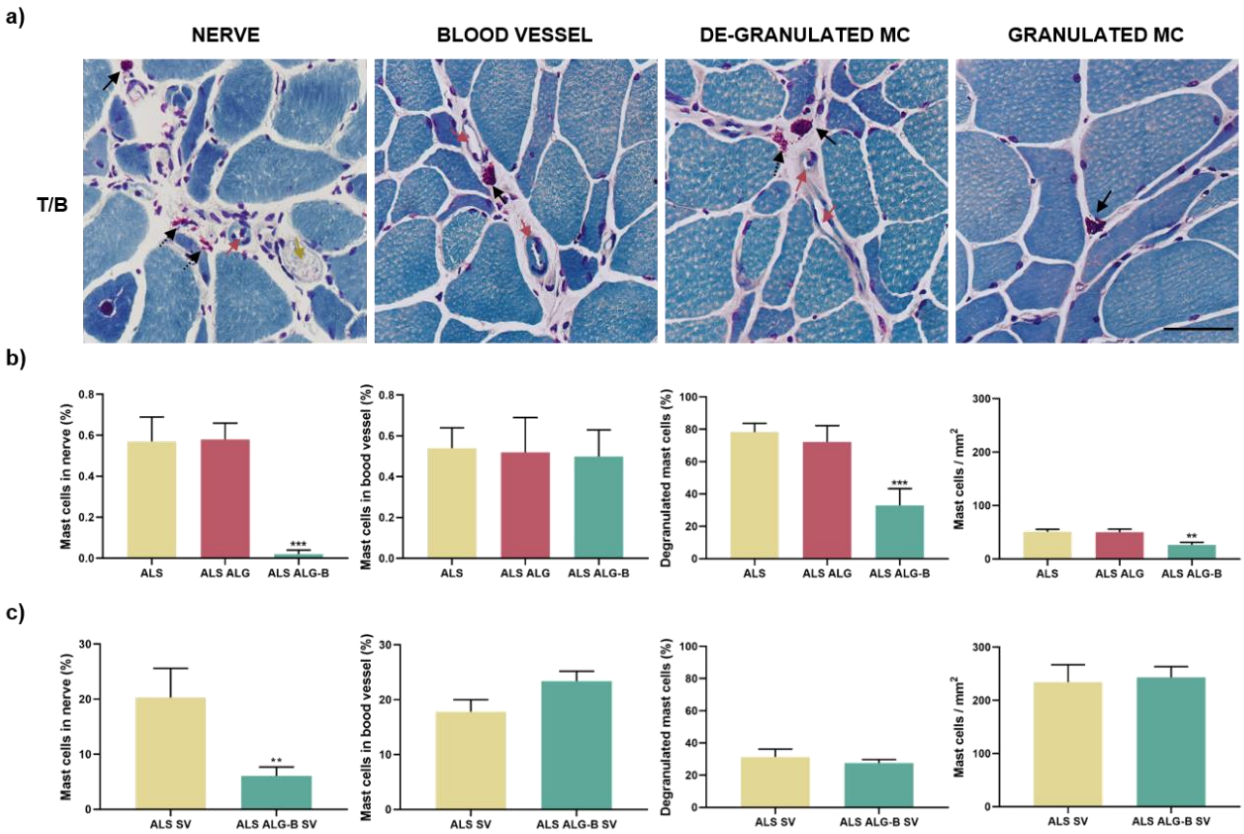

Figure 4. Infiltration and degranulation of mast cells into the skeletal muscle of pre-symptomatic and symptomatic SOD1^{G93A} mice.

(a) Analysis of mast cell recruitment in muscle by toluidine-blue staining. Quadriceps sections of pre-symptomatic **(b)** and symptomatic **(c)** mice were analysed. In both animal experiments, the ALG-B group presented a strong decrease in the density of infiltrated mast cells as well as the de-granulating mast cell number. Further, mast cells were mainly perivascular located and not close to a nerve fibre, a hallmark characteristic of extensive nerve inflammation occurring in $SOD1^{G93A}$ mice. Scale bar: 50 µm. Graphs represent the image analysis quantification of the percentage of mast cells in each location, the total number of mast cells and total number of de-granulated mast cells. Statistics are shown as mean ± standard deviation. For comparison between the 3 groups, data were analysed by an ordinary one-way ANOVA test and corrected for multiple comparisons using Tukey´s correction analysis ($p = 0.05$). For comparisons between 2 groups, data were analysed by an unpaired t-test applying Welch´s corrections ($p = 0.05$). ***$p < 0.001$. **$p < 0.01$.

However, B-treated quadriceps, in pre-symptomatic and symptomatic mice, presented a strong decrease in the density of infiltrated mast cells as well as the de-granulating mast cell number, suggesting an inhibition of mast cell migration and activation. Further, in B-treated quadriceps mast cells were mainly perivascular located and not in the close proximity to nerve fibers, suggesting that borax may downregulate mast cell-mediated inflammatory events influencing the degeneration of the muscle and the peripheral motor pathway.

We have further analyzed IL-6 muscle levels, a cytokine known for its diverse functions and crucial role in immune response, inflammation, metabolism, and hematopoiesis. When the production of IL-6 becomes dysregulated, it can lead to the development of various chronic inflammatory diseases.[52] This cytokine is produced by immune and

blood cells, endothelial cells, and myocytes during muscle contraction.[53] Interestingly, elevated levels of IL-6 have been observed in ALS patients, which is associated with motor neuron degeneration.[54] Additionally, IL-6 has been found to contribute to muscle atrophy after denervation, further highlighting the involvement of cytokines in the progression of ALS. Given its significance, IL-6 has emerged as a potential biomarker for ALS and a target for therapeutic interventions, as demonstrated by ongoing clinical trials.[55]

Figure S3 illustrates the immunofluorescence detection and image analysis quantification of IL-6 in pre-symptomatic and symptomatic mice. In both groups, the control mice exhibited elevated levels of IL-6. Notably, the IL-6 levels were significantly higher in symptomatic mice, consistent with previous findings that associate IL-6 with disease progression.[55] However, the quadriceps muscles treated with borax (ALG-B) presented reduced IL-6 levels, indicating a decrease in the inflammatory response within the muscle tissue following treatment. These findings collectively suggest that borax may function as a therapeutic agent by promoting muscle repair processes, suppressing mast cell-mediated inflammatory events, reducing pro-inflammatory cytokines such as IL-6, and mitigating muscle degeneration and neuro-inflammation.

2.5. Local muscle borax-release induces motor neuron preservation and reduces glial inflammation in spinal cord in pre-symptomatic and symptomatic SOD1^{G93A} mice.

Following the assessment of muscle inflammation, which revealed diminished inflammation specifically near muscle nerve fibers (Fig.4, S3), and the observed changes in improved motor behavior (Fig1) and improved muscle health (Fig.2, 3) that indirectly can potentially be associated with enhanced motor function or survival, we aimed to

determine if the administration of a localized muscle treatment to ALS SOD1^{G93A} mice could lead to neuroprotection.

To do that we analyzed spinal cord of pre-symptomatic and symptomatic SOD1^{G93A} mice. The SOD1^{G93A} model is characterized by motor neuron degeneration caused by the toxic effects of the SOD1 mutant protein, which affects both motor neurons and their neighboring glia.[56,57] In **Figure 5**, our findings revealed a notable and significant increase in the number of motor neurons in the spinal cord of both pre-symptomatic and symptomatic mice following local muscle treatment compared to the control groups. These results suggest that the treatment applied to the muscle tissue may have broader effects on the central nervous system in ALS, potentially influencing the neurodegenerative process and preserving motor neurons beyond the targeted muscle area. Our results are in line with previous studies indicating that preservation of muscle tissue function can slow motor neuron degeneration,[58] despite overexpression of mutant SOD1 in rodents induces a neuropathic phenotype. Furthermore, we conducted measurements to quantify the white matter area in the spinal cord. Our results indicated that pre-symptomatic mice treated with ALG-B exhibited an increased white matter area, indicating the preservation of neuronal axon integrity. These findings align with the observed reduction in inflammation shown in Figures 4 and S3. However, white matter area of symptomatic mice was similar to ALS control, despite presenting a higher number of motor neurons, indicating that axonal integrity is much compromised at the late stages of the disease.

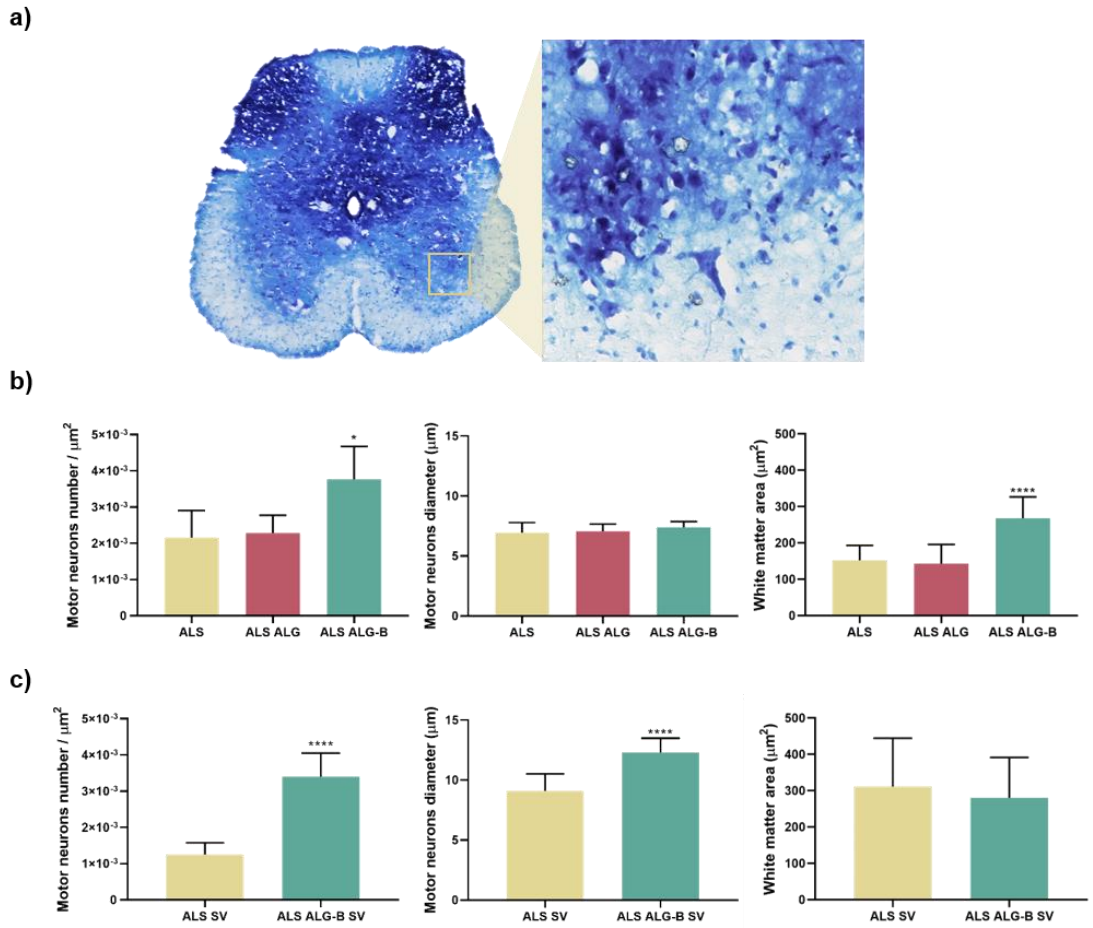

Figure 5. Evaluation of motor neuron preservation in spinal cord in pre-symptomatic and symptomatic SOD1^{G93A} mice.

a) Representative image of spinal cord stained with toluidine-blue and detail of motor neuron located in the ventral horn.

b) Number and diameter of motor neurons in the spinal cord in pre-symptomatic mice.

c) Number and diameter of motor neurons in the spinal cord in symptomatic mice.

The B treatment applied in muscle induced an increase in motor neuron number in both groups and increased motor neuron diameter in symptomatic mice.

Statistics are shown as mean ± standard deviation. For comparison between the three groups, data were analysed by an ordinary one-way ANOVA test and corrected for multiple comparisons using Tukey´s correction analysis (p = 0.05). For comparisons

between 2 groups, data were analysed by an unpaired t-test applying Welch´s corrections ($p = 0.05$). ****$p < 0.0001$, *$p < 0.05$.

In addition to the selective degeneration of motor neurons, astrogliosis is a prominent characteristic of ALS. Astrocytes, a type of glial cell, maintain neuronal homeostasis and provide support and protection for efficient neuronal function. However, in pathological conditions, activated astrocytes can have harmful effects on neuronal survival. Glial fibrillary acidic protein (GFAP) is an intermediate filament protein that is highly expressed in reactive astrocytes and is significantly up regulated in the spinal cord of ALS patients and mouse models, where reactive astrogliosis is prominent.[59] The increased production of GFAP has been linked to modulatory roles in the progression of ALS.[60] In **Figure 6**, we examined the detection of GFAP in the spinal cord of both pre-symptomatic and symptomatic $SOD1^{G93A}$ mice. Similar to the observations made regarding mast cells and IL-6 levels in muscle tissue (Figures 4, S3), we found that neuro-inflammatory levels were significantly higher in symptomatic mice, corroborating that the GFAP protein gradually increases with disease progression, consistent with previous reports.[58] Interestingly, following the local muscle treatment, we observed a reduction in GFAP values in the treated mice from both groups. These findings indicate that the application of borax in muscle has the potential to modulate neuro-inflammation processes that take place in ALS.

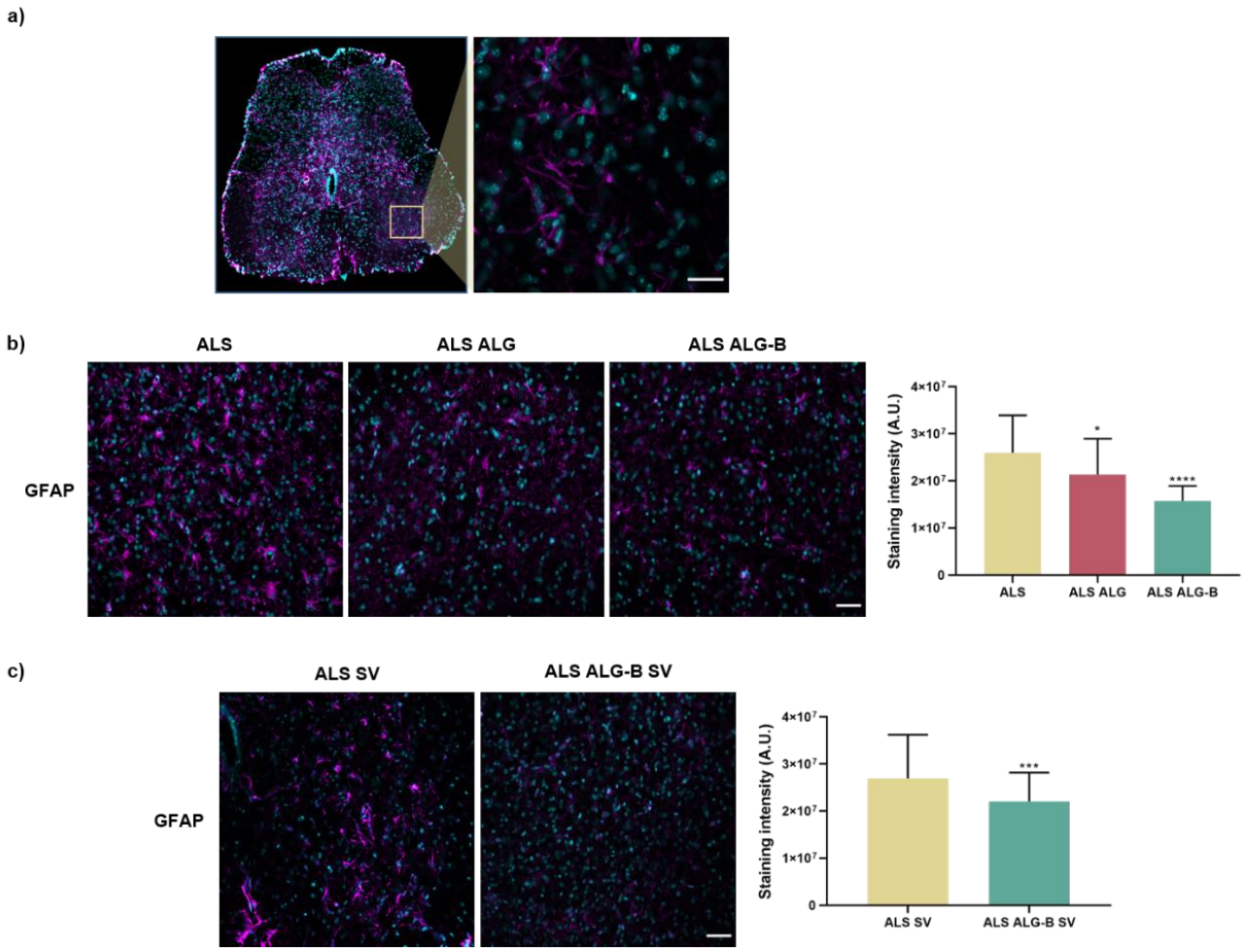

Figure 6. Evaluation of glial-mediated inflammation in the spinal cord in pre-symptomatic and symptomatic SOD1^{G93A} mice.

a) Representation of the caudal spinal cord region, with detailed ventral horn area where astrocytes are detected with GFAP antibody (magenta). Cellular nuclei were detected with DAPI. Scale bar: 20 µm.

Immunofluorescent detection of GFAP in pre-symptomatic (b) and symptomatic (c) mice. Scale bar: 50 µm. ALG-B treatment decreases GFAP expression, indicating reduction of neuro-inflammation.

Statistics are shown as mean ± standard deviation. For comparison between the three groups, data were analysed by an ordinary one-way ANOVA test and corrected for multiple comparisons using Tukey´s correction analysis (p = 0.05). For comparisons

between the two groups, data were analysed by an unpaired t-test applying Welch´s corrections ($p = 0.05$). ****$p < 0.0001$, ***$p < 0.001$, *$p < 0.05$.

3. Conclusions

This study introduces an innovative approach focused on NaBC1 activation for the regeneration of muscles affected by ALS. Our findings demonstrate that the localized application of injectable borax-loaded alginate hydrogels in the quadriceps muscles of $SOD1^{G93A}$ mice triggers NaBC1 activation, leading to enhanced muscle regeneration and repair processes. Following treatment, we observed a significant reduction of muscle inflammation, resulting in a tangible improvement in motor function and extended survival of mice. The efficacy of the treatment is further evidenced by a decline in muscle atrophy, as indicated by the decrease in slow type II fibers, diminished toxic SOD1 protein levels, and lower fibronectin levels. These outcomes, coupled with a substantial increase in active muscle satellite cells, affirm the treatment's effectiveness in promoting muscle growth, preventing muscle degeneration, and modulating inflammatory mechanisms crucial for muscle health. Notably, our study reveals that the activation of local muscle repair mechanisms induces retrograde neuroprotection by modulating neuro-inflammation, a key player in motor neuron death, ultimately preserving motor neurons.

In summary, this research provides compelling evidence supporting the involvement of muscle tissue in ALS pathology, emphasizing the potential of therapies targeting skeletal muscle for treating ALS. While ALS research typically focuses on motor neurons, the health of the muscles is paramount for overall motor function. Preserving muscle integrity through NaBC1 activation has the potential to generate neuroprotection. We propose a novel approach to decelerate neuromuscular degeneration in ALS, which may complement existing therapies targeting motor neuron inflammation.

4. Experimental section

4.1 Material substrates

Alginate-based hydrogel preparation

Ultrapure sodium alginate (FMC Biopolymer), was dissolved in 1% D-mannitol aqueous solution (Sigma-Aldrich) at a concentration of 1.5%. Borax (B) was dissolved in alginate solutions at 0.16 M concentration. Alginate solution was next filtered through a 0.22 µm pore Minisart Syringe Filter (Sartorius). For gelation, 2.7 mL of the alginate solution was mixed with 60 µL of 1.22 M $CaSO_4 \cdot 2H_2O$ (Sigma-Aldrich) through two Luer Lock syringe (BS Syringe) connected with a Fluid Dispensing Connector (Braun). Alginate and $CaSO_4 \cdot 2H_2O$ were mixed 10 times until complete homogenization. To retard the gelation time and produce injectable hydrogels, 60 µL of 0.5 M $Na_2HPO_4 \cdot 2H_2O$ (Panreac) was added to the cross-linking reaction.

Borax-release determination

The *in vitro* release of borax previous to the animal experimentation was performed by immersing the alginate-based hydrogel (ALG and ALG-B), prepared with Na_2HPO_4 at 0.5 M, in 1 mL of DPBS with Ca^{2+} and Mg^{2+} (Gibco). Hydrogels were mixed as described above and performed with identical mass and diameter (6 mm) using agarose 2% (w/v) molds. Release studies were performed simulating an 8-day cell culture in a humidified atmosphere at 37 ºC and 5 % CO_2. Aliquots consisting of the total amount of immersing liquid (1 mL) were removed from the plates after diverse time points. The reaction of the borax present in the collected aliquots with azomethine (Sigma) in an acid medium (KAc/HAc buffer pH 5.2) originates a colorimetric reaction measured at 405 nm in a Victor III (Perkin Elmer) device. Standards for calibration were prepared at

concentrations of 0, 0.1, 0.25, 0.5, 1, 1.5, 2.5, 5, 10, 25, 50 and 500 mg mL^{-1} of borax, using 40 µL aliquots from the original standard solutions for colorimetric reactions.

4.2 *In vivo* SOD1 mouse model

The experimental studies with SOD1 mice model have been conducted according to Spanish and European regulations on the use and treatment of animals (RD 223/88, RD 53/2013, and 10/13/89 OM) and the ETS-123 European Convention on the protection/welfare of vertebrate mammals used in research. Specific authorisation for the procedures were obtained (permit number 2020/VSC/PEA/0182), by the Animal Experiment Committee at Universitat Politècnica de València to ensure the avoidance of unnecessary distress, pain, harm, or suffering.

The experimental mice were housed under 12 h light / dark cycles at 23-25 ºC with relative humidity of 55 %. Food and water were available *ad libitum*. Animals were sacrificed by CO_2 inhalation.

100 µL of injectable borax-loaded ALG-based hydrogels (ALG-B, 6 mg of borax / injection) were subcutaneously injected in both quadriceps muscles at 68, 82, 96 and 110 days old *B6SJL-Tg(SOD1-G93A)1Gur/J* ALS mice. Two different experiments were performed in parallel, differing in their end point: i) mice were sacrificed at 115 days old for muscle and nerve evaluation and ii) mice were sacrificed at their final endpoint determined as the mouse´s inability to flip over within 30 seconds in the supine position (ranging between 120-146 days) for evaluation of survival (SV).

For the first experiment, three different groups of male and female mice randomly distributed were evaluated: 6 animals injected with 100 µL of saline solution as an ALS control, 6 animals with empty ALG hydrogels, and 6 animals with ALG-B hydrogels. For the survival experiment (SV), two different groups of male and female mice randomly

distributed were evaluated: 10 animals injected with 100 µL of saline solution as an ALS control and 10 animals with ALG-B hydrogels.

Changes in the body weight and motor impairment in the behavioral four-limb hanging test have been followed during the total duration of the experiments in all animals following Treat-NMD Neuromuscular Network Standard Operation Procedures (SOP, treat-nmd.org).

After euthanasia, different tissues were extracted:

- both muscle quadriceps were removed and immediately fixed in cold isopentane (-150◦ to -160 ◦C) (PanReac Applichem) for 1 min, and subsequently immersed in liquid nitrogen for 2 min. Samples were stored at -80 ºC until sectioning.
- Brain and spinal cord were removed and immediately fixed in formaldehyde 4 % during 24 h at 4 ºC, followed by cryopreservation in 30 % sucrose, inclusion in a freezing compound (OCT) and further stored at -80 ºC until sectioning.

4.3 Histology and staining

Frozen muscle, brain and spinal cord samples were sectioned using a cryostat at – 25-30 º C. 10-15 µm sections were placed on polarized slides (Superfrost, Thermofisher). Muscle histoarchitecture was evaluated by Hematoxylin-eosin staining. Muscle inflammation and motor neuron identification were determined by Toluidine Blue staining. All staining were performed following standard procedures. After sample dehydration with graded ethanol series and clearing with xylene, they were mounted with xylene-based mounting medium (Entellan, Electron Microscopy Sciences). Images were captured with a bright-field microscope (Nikon Eclipse 80i) at different magnifications.

4.4 Immunofluorescence assays

Immunofluorescence assays were performed using cryopreserved slides containing sectioned samples that were air-dry for 15 minutes at room temperature. Samples were

then permeabilized with DPBS/0.5 % Triton x-100 at room temperature for 5 min, next blocked in 2 % BSA/DPBS for 1 h at 37 ºC. Samples were then incubated with primary antibodies (**¡Error! No se encuentra el origen de la referencia.**) diluted in a blocking buffer overnight at 4 °C. The samples were then rinsed twice in DPBS/0.1 % Triton X-100 and incubated with the secondary antibody at room temperature for 1 h. Finally, samples were washed twice in DPBS/0.1 % Triton X-100 before mounting with Vectashield containing DAPI (Vector Laboratories) and images were captured under an epifluorescence microscope (Nikon Eclipse 80i) at different magnifications.

Target	Brand	Reference	Dilution
Slow Skeletal Myosin Heavy Chain	Abcam	Ab234431	1:200
SOD1	Abcam	Ab51254	1:200
PAX7	Invitrogen	PA1-117	1:200
FN	Sigma-Aldrich	F0916	1:100
GFAP	Abcam	ab7260	1:5000
IL-6	ThermoFisher	P620	1:200

Table 1. Primary antibodies used for immunofluorescence assays.

4.5 Image analysis

Muscle sequential images obtained after staining were stitched (Image Composite Editor) and segmented using Cellpose 2.0 a generalist algorithm for segmentation, allowing the identification of cell boundaries and the analysis of all fibers of a muscle cross section (2,000-5,000 fibers). This method for analyzing the entire muscle guarantees for unbiased results. Muscle histological features were identified manually and quantified using image analysis software ImageJ following Treat-NMD Neuromuscular Network Standard Operation Procedures (SOP, treat-nmd.org).

Staining intensity of immunofluorescence images were quantified by ImageJ software.

4.6 Statistics and Reproducibility

For statistical analysis GraphPad Prism 8.0.2 has been used. Data were reported as mean ± standard deviation. Normal distribution of the data was established using the D´Agostino Pearson omnibus test. Results were analysed by one-way ANOVA test with Tukey´s multiple comparison test ($p = 0.05$) when 3 or more groups were compared. Pairs of samples were compared using unpaired t-tests, applying Welch´s correction when necessary. A 95% confidence level was considered significant and is indicated by (*) $p < 0.05$, (**) $p < 0.01$, (***) $p < 0.001$, and (****) $p < 0.0001$.

Acknowledgements

Funding: PR acknowledges support by grant PID2021-126012OB-I00 funded by MCIN/AEI/10.13039/501100011033 and by ERDF a way of making Europe, and by CIBER (CB06/01/1026). JGV acknowledges the funding from the European Union-NextGenerationEU program. PR acknowledges gratefully the funding provided by the ALS patient LEP and her family and the help provided by CGR, JVH and PMN.

References

[1] J. Riancho, M. Delgado-Alvarado, M. D. Andreu, et al, *Br. J. Pharmacol.* **2021***, 178*, 1269.

[2] P. Masrori, Van Damme*, Eur. J. Neur.* **2020**, *27,* 1918.

[3] S. Penco, C. Lunetta, L. Mosca, E. Maestri, F. Avemaria, et al, *J. Mol. Neurosci.* **2011**, *44*, 25.

[4] L. Régal, L. Vanopdenbosch, P. Tilkin, L. Van den Bosch, V. Thijs, R. Sciot, W. Robberecht, *Arch. Neurol.* **2006**, *63*, 262.

[5] J. Lee, S. J. Hyeon, H. Im, H. Ryu, Y. Kim, H. Ryu, *Exp. Neurobiol.* **2016**, *25*, 233.

[6] K. K. Chand, K. M. Lee, H. Qiu, E. F. Willis, N. A. Lavidis, M. A. Hilliard, P. G. Noakes, *FASEB J*. **2018**, *32*, 2676.

[7] E. B. Moloney, F. de Winter, J. Verhaagen, *Front. Neurosci.* **2014**, *8*, 252.

[8] C. Tallon, K. A. Rusell, S. Sakhalkar, N. Andrapallayal, M. H. Farah, *Neuroscience* **2016**, *312*, 179.

[9] O. Pikatza-Menoio, A. Elicegui, X. Bengoetxea, N. Naldaiz-Gastesi, A. López de Munain, G. Gerenu, F. J. Gil-Bea, S. Alonso-Martín, *J. Pers. Med.* **2021**, *11*, 671.

[10] F. Gouel, A. S. Rolland, J. C. Devedjian, T. Burnouf, D. Devos, *Front Neurol.* **2019**, *10*, 835.

[11] G. Dobrowolny, C. Giancinti, L. Pelosi, C. Nicoletti, N. Winn, L. Barberi, M. Molinaro, N. Rosenthal, A. Musarò, *J. Cell Biol.* **2005**, *168*, 193.

[12] M. Suzuki, J. McHugh, C. Tork, B. Shelley, A. Hayes, I. Bellantuono, P. Aebischer, C. N. Svendsen, *Mol Ther.* **2008**, *16*, 2002.

[13] D. Krakora, P. Mulcrone, M. Meyer, C. Lewis, K. Bernau, G. Gowing, C. Zimprich, P. Aebischer, C. N. Svendsen, M. Suzuki, *Mol Ther.* **2013**, *21*, 1602.

[14] R. Chhabra, B. Ruozi, A. Vilella, D. Belletti, K. Mangus, S. Pfaender, T. Sarowar, T. M. Boeckers, M. Zoli, F. Forni, M. A. Vandelli, *CNS & Neurological Disorders-Drug Targets* **2015**, *14*, 1041.

[15] T. Amna, M. Shamshi Hassan, M. S. Khil, H. K. Lee, I. H. Hwang, *Surf. Interface Anal*. **2014**, *46*, 72.

[16] M. Murariu, A. Doumbia, L. Bonnaud, A. L. Dechief, Y. Paint, M. Ferreira, C. Campagne, E. Devaux, P. Dubois, *Biomacromolecules* **2011**, *12*, 1762.

[17] H. Oliveira, S. Catros, C. Boiziau, R. Siadous, J. Marti-Muñoz, R. Bareille, S. Rey, O. Castaño, J. Planell. J. Amédée, E. Engel, *Acta Biomaterialia* **2016**, *29*, 435.

[18] A. Vallejo-Illarramendi, I. Toral-Ojeda, G. Aldanondo, A. López de Munain, *Expert Rev Mol Med.* **2014**, *8*, 16.

[19] J. M. Aizpurua, J. I. Miranda, A. Irastorza, E. Torres, M. Eceiza, M. Sagartzazu-Aizpurua, P. Ferron, G. Aldanondo, H. Lasa-Fernandez, P. Marco-Moreno, N. Dadie, A. Lopez de Munain, A. Vallejo-Illarramendi, *Eur. J. Med. Chem.* **2021**, *213*, 113160.

[20] F. H. Nielsen, *J. Trace Elem. Exp. Med.* **1996**, *9*, 215.

[21] F. H. Nielsen, J. G. Penland, *J. Trace Elem. Exp. Med.* **1999**, *12*, 251.

[22] F. H. Nielsen, S. L. Meacham, *Journal of Evidence-Based Complementary & Alternative Medicine* **2011**, *16,* 169.

[23] M. Park, Q. Li, N. Shcheynikov, W. Zeng, S. Muallem, *Mol. Cell.* **2004**, *16*, 331.

[24] P. Rico, A. Rodrigo-Navarro, M. de la Peña, V. Moulisová, M. Costell, M. Salmeron-Sanchez, *Advanced Biosystems* **2018,** *3*, 1800220.

[25] P. Rico, A. Rodrigo-Navarro, L. Sánchez Pérez, M. Salmeron-Sanchez, *Communications Biology* **2020,** *3*, 717.

[26] P. Rico, A. Rodrigo-Navarro, M. Salmeron-Sanchez, *Tissue Engineering Part A* **2015**, *21*, 2662.

[27] J. Ciriza, A. Rodriguez-Romano, I. Nogueroles, G. Gallego-Ferrer, R. Martin Cabezuelo, J. L. Pedraz, P. Rico, *Materials Science & Engineering C* **2021**, *123*, 112003.

[28] M. Dadon-Nachum, E. Melamed, D. Offen, *J. Mol. Neurosci.* **2011**, *43*, 470.

[29] G. Dobrowolny, M. Aucello, E. Rizzuto, S. Beccafico et al, *Cell Metabolism* **2008**, *8*, 425.

[30] S. Oliván, A. C. Calvo, A. Rando, M. J. Muñoz, P. Zaragoza, R. Osta, *Exp. Anim.* **2015**, *64*, 147.

[31] J. D. Atkin, R. L. Scott, J. M. West, E. Lopes, A. K. J. Quah, S. S. Cheema, *Neuromuscular Disorders* **2005**, *15*, 377.

[32] L. Jensen, L. H. Jørgensen, R. D. Bech, U. Frandsen, H. D. Schrøder, *BioMed Research International* **2016**, 10.1155/2016/5930621.

[33] H. Westerblad, J. D. Bruton, A. Katz, *Experimental Cell Research* **2010**, *316*, 3093.

[34] P. F. Pradat, A. Barani, J. Wanschitz, O. Dubourg, A. Lombès, A. Bigot, V. Mouly, G. Bruneteau, F. Salachas, T. Lenglet, V. Meininger, G. Butler-Browne, *Amyotrophic Lateral Sclerosis*, **2011**, *12*, 264.

[35] S. Tsitkanou, P. A. Della Gatta, A. P. Rusell, *Front Physiol.* **2016**, *7*, 403.

[36] A. Scaramozza, V. Marchese, V. Papa, R. Salaroli, G. Sorarù, C. Angelini, G. Cenacchi, *Ultrastructural Pathology*, **2014**, *38*, 295.

[37] R. Manzano, J. M. Toivonen, A. C. Calvo, S. Olivan, P. Zaragoza, M. J. Muñoz, R. Osta, *Stem Cell Reviews and Reports*, **2012**, *8*, 279.

[38] R. Manzano, J. M. Toivonen, A. C. Calvo, S. Olivan, P. Zaragoza, M. J. Muñoz, R. Osta, *Neurodegenerative Diseases*, **2013**, *11*, 153.

[39] M. E. Gurney, H. Pu, A.Y. Chiu, M.C. Dal Canto, C.Y. Polchow, et al, *Science* **1994**, *264*, 1772.

[40] M.B. Yim, J.H. Kang, H.S. Yim, H.S. Kwak, P.B. Chock, E. R. Stadtman, *Proc. Natl. Acad. Sci. USA,* **1996**, *93*, 5709.

[41] S. Peters, E. Zitzelsperger, S. Kuespert, S. Iberl, R. Heydn, S. Johannesen, S. Petri, L. Aigner, D. R. Thal, A. Hermann, J. H. Weishaupt, T. H. Bruun, U. Bogdahn, *Frontiers in Neurology* **2017**, *8*, 669.

[42] D. Gonzalez, O. Contreras, D. L. Rebolledo, J. P. Espinoza, B. van Zundert, E. Brandan, PLoS One **2017**, *12*, e0177649.

[43] E. Trias, S. Ibarburu, R. Barreto-Núñez, V. Varela, I. C. Moura, P. Dubreuil, O. Hermine, J. S. Beckman, L. Barbeito, *JCI Insight*. **2017**, *2*, 95934.

[44] I. M. Chiu, H. Phatnani, M. Kuligowski, J. C. Tapia, M. A. Carrasco, M. Zhang, T. Maniatis, M. C. Carroll, *Proc Natl Acad Sci U S A.* **2009**, *106*, 20960.

[45] S. Wernersson, G. Pejler, *Nat Rev Immunol.* **2014**, *14*, 478.

[46] J. P. Abonia, D. S. Friend, W. G. Austen, F. D. Moore, M. C. Carroll, R. Chan, J. Afnan, A. Humbles, C. Gerard, P. Knight, Y. Kanaoka, S. Yasuda, N. Morokawa, K. F. Austen, R. L. Stevens, M. F. Gurish, *J Immunol.* **2005**, *174*, 7285.

[47] K. Ashina, Y. Tsubosaka, T. Nakamura, K. Omori, K. Kobayashi, M. Hori, H. Ozaki, T. Murata, *PLoS One* **2015**, *10*, e0132367.

[48] A. L. Christy, M. E. Walker, M. J. Hessner, M. A. Brown, *J Autoimmun.* **2013**, *42*, 50.

[49] M. Schmelz, S. Zeck, M. Raithel, R. Rukwied, *Clin Exp Allergy* **1999**, *29*, 695.

[50] E. Trias, P.H. King, Y. Si, Y. Kwon, V. Varela, S. Ibarburu, M. Kovacs, I. C. Moura, J. S. Beckman, O. Hermine, L. Barbeito, *JCI Insight*. **2018**, *3*, e123249.

[51] E. Trias, M. Kovacs, P. H. King, Y. Si, Y. Kwon, V. Varela, S. Ibarburu, I. C. Moura, O. Hermine, J. S. Beckman, L. Barbeito, *Glia* **2020**, *68*, 1165.

[52] T. Tanaka, M. Narazaki, T. Kishimoto, *Cold Spring Harb Perspect Biol.* **2014** *6*, a016295.

[53] C. Brandt, B. K. Pedersen, *J Biomed Biotechnol* **2010**, 520258.

[54] A. Pronto-Laborinho, S. Pinto, M. Gromicho, M. Pereira, M. Swash, M. de Carvalho, *J Neurol Sci*. **2019**, *398*, 50.

[55] M, Wosiski-Kuhn, J. B. Caress, M. S. Cartwright, G. A. Hawkins, C. Milligan, *Amyotroph Lateral Scler Frontotemporal Degener*. **2021**, *22*, 248.

[56] M. E. Gurney, H. Pu, A. Y. Chiu, M. C. Dal Canto, C. Y. Polchow, D. D. Alexander, J. Caliendo, A. Hentati, Y. W. Kwon, H. X. Deng, et al, *Science*, **1994**, *264*, 1772.

[57] D. Jaarsma, E. Teuling, E.D. Haasdijk, C.I. De Zeeuw, C.C. Hoogenraad, J Neurosci. **2008**, *28*, 2075.

[58] J. M. Van Dyke, I. M. Smit-Oistad, C. Macrander, D. Krakora, M.G. Meyer, M. Suzuki, *Exp Neurol*. **2016**, *277*, 275.

[59] M, Alexianu, M. Kozovska, S. Appel, *Neurology* **2001**, *57*, 1282.

[60] Y. Yoshii, A. Otomo, L. Pan, M. Ohtsuka, S. Hadano, *Neurosci Res*. **2011**, *70*, 321.